

Journal of Biomedical Optics

SPIEDigitalLibrary.org/jbo

Mesoscopic fluorescence molecular tomography of reporter genes in bioprinted thick tissue

Mehmet S. Ozturk
Vivian K. Lee
Lingling Zhao
Guohao Dai
Xavier Intes

Mesoscopic fluorescence molecular tomography of reporter genes in bioprinted thick tissue

Mehmet S. Ozturk,* Vivian K. Lee,* Lingling Zhao, Guohao Dai, and Xavier Intes

Rensselaer Polytechnic Institute, Biomedical Engineering Department, 110 8th Street, JEC#7036, Troy, New York 12180

Abstract. Three-dimensional imaging of thick tissue constructs is one of the main challenges in the field of tissue engineering and regenerative medicine. Optical methods are the most promising as they offer noninvasive, fast, and inexpensive solutions. Herein, we report the use of mesoscopic fluorescence molecular tomography (MFMT) to image function and structure of thick bioprinted tissue hosted in a 3-mm-thick bioreactor. Collagen-based tissue assembled in this study contains two vascular channels formed by green fluorescent protein- and mCherry-expressing cells. Transfected live cell imaging enables us to image function, whereas Flash Red fluorescent bead perfusion into the vascular channel allows us to image structure. The MFMT optical reconstructions are benchmarked with classical microscopy techniques. MFMT and wide-field fluorescence microscopy data match within 92% in area and 84% in location, validating the accuracy of MFMT reconstructions. Our results demonstrate that MFMT is a well-suited imaging modality for fast, longitudinal, functional imaging of thick, and turbid tissue engineering constructs. © 2013 Society of Photo-Optical Instrumentation Engineers (SPIE) [DOI: 10.1117/1.JBO.18.10.100501]

Keywords: image reconstruction; fluorescence; multispectral imaging; tissues; tomography.

Paper 130489LR received Jul. 18, 2013; revised manuscript received Sep. 15, 2013; accepted for publication Sep. 17, 2013; published online Oct. 3, 2013.

Tissue engineering is a promising technology that aims at replacing damaged tissues or organs for functional restoration.¹ Three-dimensional (3-D) bioprinting technology is capable of manufacturing thick tissues as well as printing vasculatures.² The resulting tissues are, however, thick (~3 mm), turbid, and hosted inside sealed bioreactors. Hence, it is difficult to employ traditional microscopic imaging methods to assess structure and function of the whole sample.

Optical imaging techniques, such as multiphoton or confocal microscopy, have been used in 3-D imaging of engineered tissues. Although they offer high resolution and great sensitivity, they are restricted in their penetration depth and field of view.³ For deeper imaging, optical coherence tomography (OCT) is the

main optical imaging modality due to its high resolution (1 to 15 μm) in scattering tissue at depth up to ~2 mm.⁴ OCT is inherently a structural imaging method but also extracts functional information by elucidating structural changes.^{5,6} However, even though special markers have been devised,⁷⁻¹⁰ OCT is still limited in imaging molecular probes with high sensitivity. Especially, OCT is not sensitive to fluorescence signal, extensively employed in tissue engineering.

To probe a turbid sample beyond the microscopic penetration depth, a novel method was proposed,⁹ laminar optical tomography,¹⁰ or mesoscopic fluorescence molecular tomography (MFMT), also sometimes referred to as FLOT (Ref. 11) or MEFT.¹² MFMT is able to image a few millimeters (~3 to 5 mm) thick tissues with a relatively high resolution (~100 to 200 μm).² MFMT is well suited for *in-vitro* tomographic imaging,² as well as for *ex vivo*¹² and clinical imaging scenarios.¹³ Furthermore, it can be fused with other traditional optical imaging modalities such as OCT.¹¹ One key advantage of MFMT is its ability to image a variety of fluorescent probes.

In this study, we have combined 3-D bioprinting and MFMT imaging modality. MFMT successfully retrieved the 3-D bio-distribution of the live cells, expressing reporter genes, and a perfused vascular channel. MFMT was applied through a ~3-mm-thick sealed chamber. This is a key step toward establishing MFMT as a useful imaging tool for tissue engineering applications.

MFMT imaging system is based on raster scanning a focused laser beam over the sample, Fig. 1(b). The fluorescence light is then detected at seven radial positions (d_i) away from the illumination spot in an epiconfiguration ($d_1 = 800 \mu\text{m}$, $d_7 = 3900 \mu\text{m}$).

The optical setup is similar to the one in Zhao et al.² We have replaced the lenses with antireflective-coated achromatic ones and added one spectral channel. We have used emission filters (XB97/560BP10, Omega Optics; FF01-650/60-25, and FF01-700/13-25, Semrock) for corresponding Diode Laser source of 488, 589, and 658 nm, respectively. The focused beam impinges 17 mW on a circular area of 375 μm diameter on the chamber.

Emission signal and a matching background signal were acquired during raster scanning of the flow chamber over $3 \times 7 \text{ mm}^2$ area, $x - y$. The dwelling time at each collected source point was ~8.3 μs . The $3 \times 7 \text{ mm}^2$ area imaged in this work lead to 80×200 source positions ($\Delta x = 37 \mu\text{m}$; $\Delta y = 35 \mu\text{m}$) and a total acquisition time of ~132.8 ms/frame (16,000 source position; corresponds to ~7.5 fps frame rate). Data acquisition was averaged over 1 min (~450 frames) to obtain fluorescent data with good signal-to-noise ratio. The averaged background signal was subtracted from averaged emission signal to minimize the autofluorescence and the bleed-through effect *a posteriori*. Reconstructions were performed using 14,400 laser beam positions, as artifacts originated from the software were observed on the border of the imaging area. Overall, the 14,400 source positions and data gathered from seven detectors for each laser beam position led to a total of 100,800 spatial data points. We used a CPU-based Monte Carlo photon propagation model to compute the Jacobian matrix. The forward simulations were carried with 10^5 photons and $0.2 \times 0.2 \times 0.2 \text{ mm}^3$ voxels. The optical properties, used to compute the Jacobian, were set at $\mu_s = 5 \text{ mm}^{-1}$,

*These authors contributed equally to this work.

Address all correspondence to: Xavier Intes, Rensselaer Polytechnic Institute, Biomedical Engineering Department, 110 8th Street JEC#7036 Troy, New York 12180. Tel: 518-276-6964; Fax: 518-276-3035; E-mail: intesx@rpi.edu

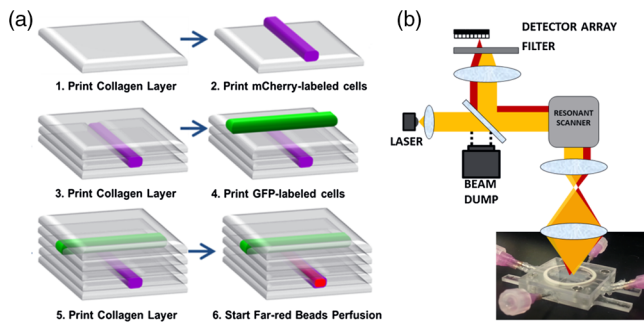


Fig. 1 (a) Three-dimensional (3-D) bioprinting steps are depicted. Lower (purple) channel is mCherry. Upper (Green) is green fluorescent protein (GFP) channel. Lower (Red) in final step represents far-red fluorescent beads for perfusion. (b) Excitation signal (solid yellow) raster scanned over the sealed chamber. Emission signal (solid red) descanned and imaged on to detectors after filtering excitation signal.

$\mu_a = 0.002 \text{ mm}^{-1}$, and $g = 0.9$. These values were selected based on previous studies² and reported values for collagen in the literature. Note that the optical properties were similar for all wavelengths investigated herein.

Human umbilical vein endothelial cells (HUVEC) were labeled with three different colors: GFP ($\lambda_{ex}/\lambda_{em} = 488/507 \text{ nm}$), mCherry ($\lambda_{ex}/\lambda_{em} = 587/610 \text{ nm}$), and far-red ($\lambda_{ex}/\lambda_{em} = 650/670 \text{ nm}$). Reporter genes were used for GFP and mCherry labeling (lentiviral transfection). For far-red, HUVECs were labeled with $5 \mu\text{M}$ far-red cell tracker [DiIC18(5)-DS, Invitrogen, Grand Island, New York]. The labeled cells were cultured at 37°C in $5\% \text{ CO}_2$ in endothelial cell growth medium-2 (Lonza, Allendale, New Jersey).

To validate the MFMT capability on reconstructing complex structures, “R,” “P,” “I,” 2-D letters were printed on collagen matrix (type I, 3.0 mg/mL , BD Bioscience, San Jose, California) [Fig. 2(a)]. Far-red, GFP, and mCherry-labeled HUVECs were used to print ‘R’, ‘P’, and ‘I,’ respectively.

Through a layer-by-layer approach, two vascular channels were constructed inside of a 3-mm-thick sealed chamber (Fig. 1).^{1,2} GFP- and mCherry-expressing cells were seeded on the inner surface of top and bottom channels, respectively.

The distance between orthogonally located channels was varied (100 and $1300 \mu\text{m}$) to test the imaging capability in different configurations. To visualize the channel structure, Flash Red beads (Bangs Laboratory Inc.) were perfused into the lower channel (mCherry cells seeded) at 0.1 mL/min flow rate.

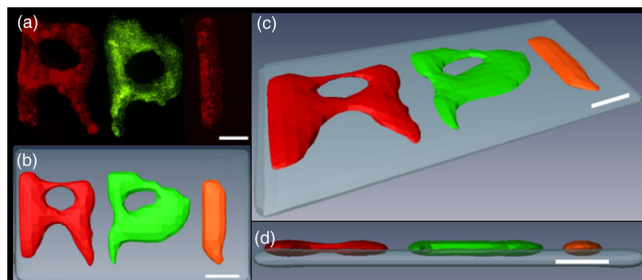


Fig. 2 (a) Fluorescent wide field microscopy (FWFM) image of R, P, I letters is expressing, Far-red cell tracker, GFP and mCherry, respectively. 3-D reconstruction is shown from top (b), from perspective (c) and side view image (d) shows the letters printed on the top of the collagen block sample (thin sample). Results show the accuracy of MFMT reconstruction as it is benchmarked against FWFM. Scale bar, 1 mm .

We benchmarked the 3-D reconstructions (RECONS) against two classical microscopic modalities (via maximum intensity projection): phase contrast microscopy (PCM) and fluorescent wide field microscopy (FWFM) (Eclipse Ti, Nikon). Accuracy of the reconstruction was quantified by segmentation of FWFM, PCM, and reconstruction images by an ImageJ plugin (mixture modeling). Two metrics for objective image analysis were derived: area of segmented image (mm^2) and agreement factor (AF). First, areas ($A_{\text{FWFM}}, A_{\text{PCM}}, A_{\text{RECONS}}$) and area ratios ($A_{\text{RECONS}}/A_{\text{FWFM}}$ and $A_{\text{RECONS}}/A_{\text{PCM}}$) were calculated. Then, overlap ratio was estimated: $(A_{\text{RECONS}} \cap A_{\text{FWFM}})/A_{\text{RECONS}}$ and $(A_{\text{RECONS}} \cap A_{\text{PCM}})/A_{\text{RECONS}}$. Both area ratio and overlap ratio were lumped together in the AF: $\text{AF} = 2/(|1 - \text{Area ratio}| + |1 - \text{Overlap ratio}|)$. If both the areas and locations, between modalities matched, $\text{AF} = 1$.

MFMT successfully reconstructed the printed patterns regardless of the spectral range (green, red, and far-red) and labeling methods (cell tracker and reporter genes) [Fig. 2(a)]. The MFMT reconstruction results [Figs. 2(b)–2(d)] matched the wide field images, demonstrating the ability of MFMT to recover the shape of the letters with accuracy. Area values for FWFM, PCM, and MFMT reconstruction are: $6.3, 6.86, 4.6 \text{ mm}^2$ for ‘R’; $5.44, 5.97, 4.33 \text{ mm}^2$ for ‘P’; $1.63, 2.78, 1.98 \text{ mm}^2$ for ‘I’. AF values of ‘R’, ‘P’, ‘I’ are $1.33, 1.31,$ and 1.25 .

Two-channel collagen structures formed with varying channel-to-channel distance were constructed: orthogonal channels were printed closely ($\sim 100 \mu\text{m}$), and far apart ($\sim 1.3 \text{ mm}$). In PCM imaging, the channels exhibited elliptic cross-sections estimated to be around 0.7 to 1.3 mm in width and 0.4 to 0.8 mm in height. Reconstruction for both cases and benchmarking against PCM and FWFM images are depicted in Figs. 3 and 4. The populations of GFP and mCherry cells were distinguished accurately in both cases. Channels were estimated to be 0.8 to 1 mm in width and 0.6 to 0.8 mm in height for GFP and mCherry, respectively (Fig. 3). Far apart channels had a width of 1.55 mm and 1.1 mm for GFP and mCherry, respectively, and a height of $\sim 0.5 \text{ mm}$ for both (Fig. 4). Overall, these dimensions were consistent with the values estimated by PCM. However, changes in temperature or

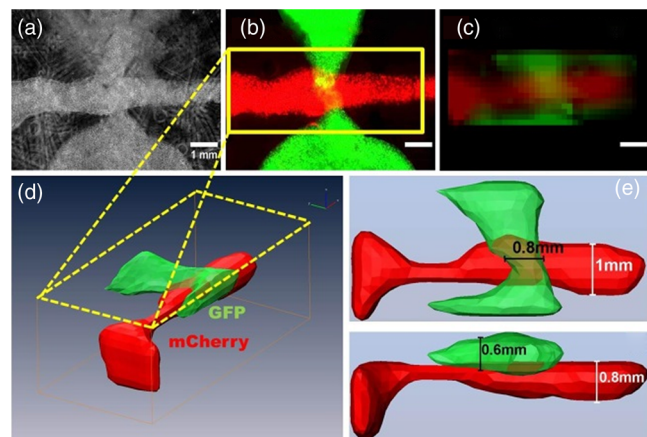


Fig. 3 Phase contrast microscopy (PCM) (a) and FWFM image (GFP is green, mCherry is red) (b). Maximum intensity projections of MFMT reconstructions were merged (c). 3-D perspective image (d), top view (e) and side view (f) images, obtained from MFMT, show the position of vascular channels. GFP and mCherry channels are printed adjacent in 0.5 mm and 1 mm in depth, respectively. Scale bar, 1 mm .

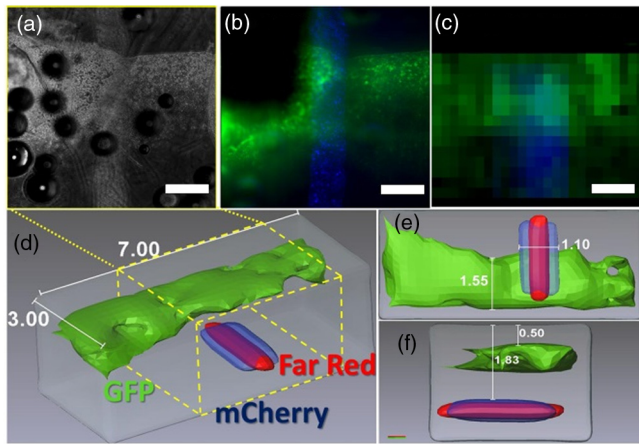


Fig. 4 PCM (a) and FWF image (GFP is green, mCherry is blue) (b). Maximum intensity projections of actual images were merged (c). 3-D perspective image (far-red is red) (d), bottom view and front view (f) images show the position of vascular channels. GFP and mCherry channels were printed in 0.5 and 2 mm, respectively. Black square in (b) is a FWF defect that occurred while acquiring the data. PCM image provides us the location for GFP-expressing cells in that same location. Scale bar, 1 mm.

inner-channel pressure caused slight expansion at channel edges, so this expansion also appeared in the MFMT reconstruction edges. Area values for FWF, PCM, and reconstruction are: 3.93, 3.31, and 4.09 mm² for GFP; 6.13, 7.43, and 5.75 mm² for mCherry. AF values for FWF and PCM are: 1.21, 1.49 for GFP and 1.16, 1.29 for mCherry. FWF images are in better agreement with reconstruction values. This is an expected outcome as both FWF and reconstruction are sensitive to the same contrast function.

Additionally, Flash Red fluorescent beads perfusion through lower channel (mCherry) was reconstructed in 3-D (Fig. 4). The reconstructed beads flow was colocalized with lower channel reconstruction [Figs. 4(d)–4(f)]. mCherry and beads flow reconstruction showed a slight discrepancy in the overall size. This may be due to the beads' accumulation on the centerline of the channel during gentle beads perfusion (0.1 mL/min). The problem can be addressed by applying a higher flow rate or using larger beads. A slight overlap was observed where two channels are adjacent (~100 μm) (Fig. 3), and this is attributed to voxel size of 200 μm. With higher computational cost, the voxel size can be decreased to increase the image space resolution and, hence, separate channels more accurately. We also note that the optical properties were kept constant for all reconstructions. Hence, a slight mismatch between true and simulated optical properties over the spectral range of the system was induced. The impact of optical property mismatch between the light propagation model and the sample has been studied for diffuse optical tomography (Ref. 14) and we are currently investigating the effect of this mismatch on MFMT performance. We expect it to be the main source of mismatch between microscopy and MFMT reconstructions observed in this study.

In this study, we have demonstrated 3-D fluorescence reconstruction of live, reporter gene expressing cells, and

perfusion through vascular channels in 3-mm engineered tissue constructs within a (this can be also performed via Doppler OCT) bioreactor. The whole imaging, data acquisition and reconstruction, was completed in less than 5 min for each fluorophore.

Our results, as well as the previous studies,² show the potential of MFMT as a powerful tool for tissue engineering applications. We believe that MFMT will have an important role to localize and monitor live fluorescent cells in thick tissue. This is a cost- and time-effective technique to evaluate the dynamic progression and functional status of engineered tissues prior to host implantation. In future studies, we plan to employ this technique to assess the maturation process of printed vasculature as well as *in-vivo* imaging.

Acknowledgments

This work was partly funded by the American Heart Association Scientist Development Grant SDG12050083, National Institutes of Health grant R21 HL102773 and NSF CAREER AWARD CBET- 1149407, NSF CBET-1263455.

References

1. W. Lee et al., "On-demand three-dimensional freeform fabrication of multi-layered hydrogel scaffold with fluidic channels," *Biotechnol. Bioeng.* **105**(6), 1178–1186 (2010).
2. L. Zhao et al., "The integration of 3-D cell printing and mesoscopic fluorescence molecular tomography of vascular constructs within thick hydrogel scaffolds," *Biomaterials* **33**(21), 5325–5332 (2012).
3. E. Hoover and J. Squier, "Advances in multiphoton microscopy technology," *Nat. Photonics* **7**(2), 93–101 (2013).
4. J. G. Fujimoto, *Optical Coherence Tomography, Technology and Applications*, pp. 1, Springer, New York (2011).
5. W. Tan et al., "Structural and functional optical imaging of three-dimensional engineered tissue development," *Tissue Eng.* **10**(11–12), 1747–1756 (2004).
6. R. Leitgeb et al., "Real-time measurement of in vitro flow by Fourier-domain color Doppler optical coherence tomography," *Opt. Lett.* **29**(2), 171–173 (2004).
7. A. L. Oldenburg, J. R. Gunther, and S. A. Boppart, "Imaging magnetically labeled cells with magnetomotive optical coherence tomography," *Opt. Lett.* **30**(7), 747–749 (2005).
8. K. D. Rao et al., "Molecular contrast in optical coherence tomography by use of a pump-probe technique," *Opt. Lett.* **28**(5), 340–342 (2003).
9. A. Dunn and D. Boas, "Transport-based image reconstruction in turbid media with small source-detector separations," *Opt. Lett.* **25**(24), 1777–1779 (2000).
10. E. M. C. Hillman et al., "Laminar optical tomography: demonstration of millimeter-scale depth-resolved imaging in turbid media," *Opt. Lett.* **29**(14), 1650–1652 (2004).
11. S. Yuan et al., "Three-dimensional coregistered optical coherence tomography and line-scanning fluorescence laminar optical tomography," *Opt. Lett.* **34**(11), 1615–1617 (2009).
12. S. Björn, V. Ntziachristos, and R. Schulz, "Mesoscopic epifluorescence tomography: reconstruction of superficial and deep fluorescence in highly-scattering media," *Opt. Express* **18**(8), 8422–8429 (2010).
13. T. J. Muldoon et al., "Analysis of skin lesions using laminar optical tomography," *Biomed. Opt. Express* **3**(7), 1701–1712 (2012).
14. X. Cheng and D. Boas, "Systematic diffuse optical image errors resulting from uncertainty in the background optical properties," *Opt. Express* **4**(8), 299–307 (1999).